Proceedings of the ASME 2020 Dynamic Systems and Control Conference
DSCC 2020
October 4-7, 2020, Pittsburgh, Pennsylvania, USA

DSCC2020-3124

TEMPERATURE SENSOR DEPLOYMENT FOR SCALABLE BATTERY PACKS

Mengzhu Gao, Qingzhi Lai and Xinfan Lin*
Department of Mechanical and Aerospace Engineering
University of California, Davis, California 95616
Email: mzga, qlai and lxflin @ucdavis.edu

ABSTRACT

Li-ion battery systems have been widely used as an essential power source in many applications. To ensure the safety and longevity of the system, a battery pack thermal model is often used in combination with distributed temperature sensors for thermal management and monitoring purposes. Due to the limited number of sensors and sparse measurement, sensor deployment to maximize the observability of the system thermal dynamics has been a critical topic, which has attracted research attention but remains to be resolved. This paper is devoted to exploring the pattern of optimal sensor locations for scalable battery systems under different observability criteria. A battery pack thermal model is first developed based on a single cell thermal model and considering the thermal interconnection between cells in the pack. Sensor location optimization is then performed by maximizing two Gramian-based observability metrics, which quantify different aspects of system observability. Optimal sensor locations obtained under the two metrics are analyzed and compared for battery systems of different sizes. Based on the results, deployment patterns of optimal sensor locations are extracted and analyzed theoretically by correlating to the physics of the battery thermal dynamics. Moreover, the influences of critical parameters of battery packs on system observability are also analyzed and discussed.

1 INTRODUCTION

Lithium-ion batteries have been widely used in many fields, such as electric vehicles (EV) [1, 2], unmanned aerial vehicles (UAV) [3], and spacecraft [4] among others, as the energy source or storage system due to their advantages in energy density, durability, and zero-emission. During operation, the temperatures of the battery pack/system will increase because of the internal chemical reactions and thermal dynamics. To ensure operational safety and battery longevity, it is desirable to limit the battery temperature and temperature rise within a certain range.

The capability of monitoring the thermal behavior of a battery system with high accuracy is essential to battery thermal management. However, temperature monitoring is typically challenging, because the battery system, especially those in EVs, typically consists of a large number of battery cells, of which the temperature evolution and distribution are governed by the thermal dynamics of single cells as well as the thermal interconnection between cells. To tackle this challenge, model-based estimation has been studied extensively in literature [5]. In many cases, a thermal model of the battery system is combined with available temperature sensors to generate accurate and robust estimation of battery temperature and/or temperature distribution. For example, in [6], a closed-loop observer is designed to estimate the core and surface temperatures of each cell in a cylindrical battery string. The estimation was based on a lumped-state battery-string thermal model and surface temperature measurement of some cells in the string. In [7], similar approaches are applied to a prismatic cell string. In [8], the temperature profile across a string of three prismatic cells was reconstructed based on a 3-D battery thermal model and surface temperature measurements of every cell. Furthermore, robust estimation of battery system temperature under sparse sensing has also been studied in [9, 10].

For all these works on battery system temperature estimation, the locations of temperature sensors, which are typically

*Corresponding author.

installed on the surface of a limited number of cells [11], have critical impact on the estimation results. Specifically, the sensor locations determine the observability of the thermal system, which is directly related to the stability, accuracy, converging speed, and robustness of the estimation results [6]. Therefore, sensor deployment strategies for a battery cell or a string of batteries have been investigated in literature. Specifically, in [6], the rank of the observability matrix is used to determine the minimum number of sensors and their locations needed to guarantee the observability of a 1-D cylindrical battery string. In [12], different metrics of the observability gramian, which is an energy-related measure of observability, are used as criteria for sensor deployment of the same battery string. Similar work has been performed in [7] for battery systems consisting of strings of prismatic cells. In [9, 10], the optimal sensor location for a string of 10 cells is determined based on the worst-case estimation error under model uncertainty. In [13], the modal observability is defined from the eigen-decomposition of a PDE-based battery system thermal model and then used to determine the optimal sensor locations. Although these works have made important contributions to the area of temperature sensor deployment for battery systems, there are several critical gaps that need to be filled. First, existing studies are mostly limited to 1-D battery strings, which may not be representative of the actual battery system configuration. Second, most works did not look into the pattern of optimal sensor locations that are generalizable to scalable battery systems with varying sizes. In addition, the relationship between observability and critical system parameters is also largely unexplored.

This paper is devoted to exploring the pattern of optimal sensor locations for scalable battery systems under different observability criteria. A scalable model is first developed to capture the thermal dynamics of a typical 2-D battery system consisting of various rows and columns of cylindrical battery cells. The model is based on a single cell thermal model [14] and considers the thermal interconnection between cells including cell-to-cell heat conduction and coolant flow convection dynamics [6]. The observability of the battery thermal system is measured in terms of the observability Gramian. Specifically, the trace and smallest eigenvalue of the observability Gramian are used as two metrics to quantify observability. The former reflects the average observability among all directions in the state space, while the latter measures the obserability of the least observable direction [15]. Optimal sensor locations obtained by optimizing these two metrics are compared for battery systems with different sizes. Patterns of optimal sensor locations are extracted from the results, and analyzed theoretically by correlating to the physics of the battery thermal system. Furthermore, the influence of the battery system parameters, including cell to cell thermal conduction resistance and cell spacing, on the two metrics and sensor deployment patterns are also analyzed and discussed.

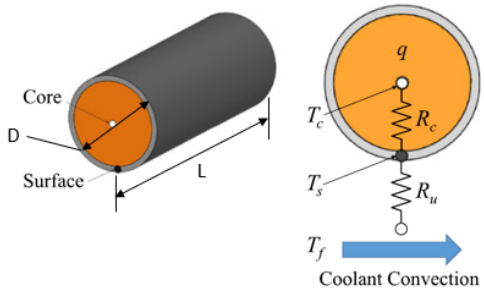

FIGURE 1: Battery thermal model for single cell [14]

2 BATTERY SYSTEM THERMAL MODEL

2.1 Single cell thermal model

The single-cell battery thermal model used here is adopted from [1, 14], as shown in Fig. 1. The surface temperature T_s and core temperature T_c are the two states of the thermal model, and T_f is the coolant flow temperature, which is regarded as an input. The thermal dynamics of the cell can be described by the following equations,

$$\begin{aligned} C_c \frac{dT_c}{dt} &= I^2 R_e + \frac{T_s - T_c}{R_c} \\ C_s \frac{dT_s}{dt} &= \frac{T_f - T_s}{R_u} - \frac{T_s - T_c}{R_c}, \end{aligned} \tag{1}$$

where R_e is the battery internal electrical resistance governing the Joule heat generation together with the input current I; R_c is the conduction resistance related to the heat conduction between the core and surface of the battery; C_c and C_s are the heat capacities of the core and surface of the battery; and R_u is the convection resistance related to the heat convection between the surface of the battery and coolant flow. More specifically, R_u takes the form [16, 17]

$$R_u = \frac{1}{\left(\rho \dot{V} c_p\right)_f \left(1 - e^{-NTU}\right)}. \tag{2}$$

In this equation, ρ is the coolant density, c_p is the isobaric specific heat of the coolant, and $\dot{V}$ is the coolant flow rate around the cell calculated as

$$\dot{V} = S_T L v, \tag{3}$$

where v is the flow velocity, L is the length of the battery, and S_T is the spacing between the center of two adjacent cells as showed

in Fig. 2. In addition, NTU is the number of transfer unit given by

$$NTU = \frac{\pi Nu_D k_f L}{\left(\rho \dot{V} c_p\right)_f} \tag{4}$$

D is the diameter of the cell, k_f is the thermal conductivity of coolant flow, and Nu_D is the Nusselt number,

$$Nu_D = C_1 Re_{D,\max}^m Pr^{0.36} \left(\frac{Pr}{Pr_s}\right)^{1/4}. \tag{5}$$

In Eqn. (5), C_1 and m are factors depending on the configuration of pack [17], v_{max} is the the maximum flow velocity around the cell,

$$v_{\max} = \frac{S_T}{S_T - D} v, \tag{6}$$

$Re_{D,\max}$ is the Reynolds number at the maximum velocity

$$Re_{D,\max} = \frac{V_{\max} D}{\nu}, \tag{7}$$

ν is the kinematic viscosity of the coolant, Pr is the Prandtl number of the coolant, and Pr_s is the Prandtl number of the coolant at the surface temperature of cell.

It is noted that the cell spacing S_T is an important geometric parameter for pack design.

2.2 Battery pack configuration and system thermal model

The configuration of a typical battery pack consisting of m rows and n columns of cells considered in this paper is shown in Fig. 2. The thermal dynamics of a cell at the ith row and jth column, i.e. cell ij, can be established by combining the single cell thermal model in Eqn. (1) with the thermal interconnection between cells,

$$\begin{aligned} C_c \frac{dT_{c,ij}}{dt} &= I^2 R_e + \frac{T_{s,ij} - T_{c,ij}}{R_c} \\ C_s \frac{dT_{s,ij}}{dt} &= \frac{T_{f,ij} + T_{f,(i+1)j} - 2T_{s,ij}}{R_u} - \frac{T_{s,ij} - T_{c,ij}}{R_c} + Q_{cc,ij}. \end{aligned} \tag{8}$$

In Eqn. (8), $Q_{cc,ij}$ is the heat conduction between adjacent cells, e.g. through the tab connecting cells or the air gap in between. It can be calculated as

$$Q_{cc,ij} = \sum_k^N \frac{T_{s,k} - T_{s,ij}}{R_{cc}} = \sum_k^N \frac{T_{s,k}}{R_{cc}} - N\frac{T_{s,ij}}{R_{cc}} \tag{9}$$

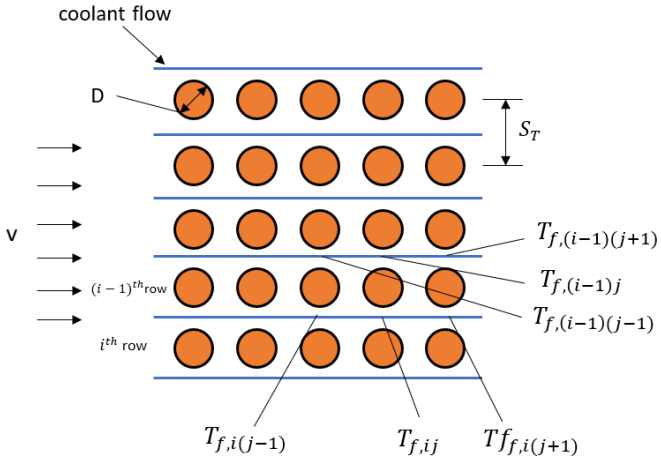

FIGURE 2: Battery pack configuration

where $T_{s,k}$ represents the surface temperature of each adjacent cell of cell ij. It is noted this term differs for cells at different location of the pack, i.e. $N = 2$ for cells at the corners, $N = 3$ for the other cells at the first and last rows and columns, and $N = 4$ for cells in the middle of the pack. The heat conduction resistance R_{cc} is an important pack parameter reflecting the thermal connection between cells, whose value is dependent on pack configuration and materials [18].

The term $\frac{T_{f,ij}+T_{f,(i+1)j}-2T_{s,ij}}{R_u}$ represents the heat convection between the surface of cell ij and the coolant flow around the upper side of the cell (with temperature $T_{f,ij}$) and that around the lower side (with temperature $T_{f,(i+1)j}$) as shown in Fig. 2. The flow rate in Eqn. (3) here is $\dot{V} = S_T L v/2$. It is noted that the coolant temperature T_f will vary at different locations of the pack governed by the flow thermal dynamics,

$$T_{f,ij} = T_{f,i(j-1)} + \sum_k^N \frac{T_{s,k} - T_{f,i(j-1)}}{R_u C_f}, \tag{10}$$

which indicates that the coolant temperature increases as it picks up heat from the cells along its path. In Eqn. (10), C_f is the heat capacity of the coolant flow which depends on the type of the coolant and the flow rate, and $T_{s,k}$ represents the surface temperature of each cells around the flow, which differs at different location of the pack, i.e. $N = 0$ for the flow around the cells at the first column (equal to the inlet flow temperature $T_{f,in}$), $N = 1$ for that around the other cells at the top and bottom row, and $N = 2$ for that in the middle of the pack.

Based on Eqns. (8-10), a state space model

$$\begin{aligned} \dot{x} &= Ax + Bu \\ y &= Cx + Du \end{aligned} \tag{11}$$

of the battery system thermal dynamics can be constructed, where the states x consist of the surface and core temperatures of all the cells in the string,

$$x = \left[T_{c,11}\ T_{s,11}\ T_{c,12}\ T_{s,12}\ \cdots\ T_{c,mn}\ T_{s,mn}\right]^T, \tag{12}$$

and the state matrix A is shown in Eqn. (13). The outputs y represent the temperature measurements available in the battery system, which are the surface temperatures of the cells with sensors,

$$y = \left[T_{s,s1}\ T_{s,s2}\ \cdots\ T_{s,sM}\right]^T. \tag{14}$$

The subscript $_{si}$ denotes the index of the cell with a sensor, and M is the total number of sensors. The output matrix will hence take the form

$$C = \begin{bmatrix} 0\cdots 0\ 1\ 0\cdots 0\ 0\ 0\cdots \\ 0\cdots 0\ 0\ 0\cdots 0\ 1\ 0\cdots \end{bmatrix}, \tag{15}$$

in which the elements 1's locate at even entries corresponding to the surface temperature of the cells with sensors, and the rest of the elements are 0. Since only the state matrix A and the output matrix C are needed for observability analysis and sensor deployment, other variables and matrices are not discussed here.

3 SENSOR DEPLOYMENT METHODOLOGY

3.1 Observability Gramian-based criteria

Rather than the Kalman's observability matrix rank condition which gives a binary determination of whether or not the system is observable, the observability Gramian is an observable criteria that provides a quantification of the system observability.

For a stable system (as the battery thermal model is), the observability gramian is defined as [19]

$$W_o = \int_0^\infty e^{A^T t} C^T C e^{At} dt, \tag{16}$$

which is a symmetric positive-semidefinite matrix. It can be shown that the observability gramian is related to the energy contained in the output of the system E_o excited by the initial state x_0 [19],

$$E_o = \int_0^\infty ||y(t)||_2^2 dt = x_0^T W_o x_0. \tag{17}$$

Mathematically, W_o needs to be invertible/positive-definite for the system to be observable. Furthermore, W_o also provides a way to quantify the relative degree of observability. Intuitively, the higher the output energy E_o (excited by x_0) is, the easier it is to observe x_0 from the output, hence indicating stronger observability. Following this line of thought, E_o can be decomposed as

$$E_o = \sum_{i=1,\ldots,n} \lambda_i \left(\mathbf{v}_i \cdot \mathbf{x}_0\right)^2, \tag{18}$$

where λ_i's are the eigenvalues of W_o, $\mathbf{v}_i$'s are the associated eigenvectors which are orthogonal to each other, and $\mathbf{v}_i \cdot \mathbf{x}_0$ is the projection of x_0 on each $\mathbf{v}_i$. Eqn. (18) quantifies the observability along different directions of the state space partitioned by $\mathbf{v}_i$. Specifically, $\mathbf{v}_i$ associated the largest λ_i indicates the most observable direction, while that associated with the smallest λ_i shows the least observable one, and the value of λ_i represents the degree of observability along each $\mathbf{v}_i$.

With the above basic understanding, various scalar metrics of W_o can be used as the criteria to evaluate the system observability under different sensor deployments [15]. For example, the trace of W_o, $tr(W_o)$, which is the sum of its diagonal elements as well as the sum of λ_i's,

$$\mathrm{tr}\left(W_o\right) = \sum_{i=1}^{n} diag(W_o)_i = \sum_{i=1}^{n} \lambda_i\left(W_o\right), \tag{19}$$

quantifies the total/average observability (output energy) along all directions in the state space; and the smallest eigenvalue, λ_{min},

$$\lambda_{min} = \min_i \lambda_i(W_o) \tag{20}$$

measures the weakest observability among all directions. These two metrics will be used for optimizing the sensor locations in this work.

3.2 Formulation of Sensor Deployment Problem

The optimal sensor deployment problem for a battery system can be formulated as a set function optimization problem. Specifically, the goal is to find the sensor locations S, which will give the output matrix $C(S)$ that maximizes the gramian-based

$$A = \begin{bmatrix} \frac{-1}{R_cC_c} & \frac{1}{R_cC_c} & 0 & 0 & 0 & 0 & \cdots & 0 & 0 & 0 \\ \frac{1}{R_cC_s} & \frac{-1}{C_s}(\frac{2}{R_u}+\frac{1}{R_c}+\frac{2}{R_{cc}}) & 0 & \frac{1}{R_{cc}C_s} & 0 & 0 & \cdots & 0 & 0 & 0 \\ 0 & 0 & \frac{-1}{R_cC_c} & \frac{1}{R_cC_c} & 0 & 0 & \cdots & 0 & 0 & 0 \\ 0 & \frac{1}{C_s}(\frac{2}{R_u^2C_f}+\frac{1}{R_{cc}}) & \frac{1}{R_{c,12}C_s} & \frac{-1}{C_s}(\frac{2}{R_u}+\frac{1}{R_c}+\frac{3}{R_{cc}}) & 0 & \frac{1}{R_{cc}C_s} & \cdots & 0 & 0 & 0 \\ & & & & & \ddots & & & & \\ 0 & 0 & 0 & 0 & 0 & 0 & \cdots & 0 & -\frac{1}{R_cC_c} & \frac{1}{R_cC_f} \\ 0 & 0 & 0 & 0 & 0 & 0 & \cdots & \frac{1}{C_s}(\frac{2}{R_u^2C_f}+\frac{1}{R_{cc}}) & \frac{1}{R_uC_s} & \frac{-1}{C_s}(\frac{2}{R_u}+\frac{1}{R_c}+\frac{2}{R_{cc}}) \end{bmatrix} \tag{13}$$

observability metric $f(W_o(A,C(S)))$,

$$\begin{aligned} &\max_S f(W_o(A,C(S))) \\ &s.t. \quad S \in \mathbf{S} \end{aligned} \tag{21}$$

where $\mathbf{S}$ is the set of all possible combinations of sensor locations, and $f(W_o)$ can be the trace, smallest eigenvalue or other metric of W_o. The C matrix takes the form in Eqn. (15), where the locations of elements 1 are specified by the sensor locations S.

To evaluate the cost function for a specific output matrix C, the observability Gramian can be calculated by solving the following Lyapunov equation,

$$A^T W_o + W_o A = -C^T C. \tag{22}$$

To find the optimal C, certain properties of the metrics of W_o can be explored to facilitate the solution by avoiding exhaustive search. Specifically, $tr(W_o)$ has been proven to be modular in [15]. This means that given a set of M sensors located at different cells yielding a C matrix with M rows,

$$C = \begin{bmatrix} C_1 \\ C_2 \\ \cdots \\ C_k \\ \cdots \\ C_M \end{bmatrix}, \tag{23}$$

where each C_k corresponds to one sensor, the total $tr(W_o(A,C))$ under C is equal to the sum of $tr(W_o(A,C_i))$ under each C_i,

$$tr(W_o(A,C)) = \sum_{i=1}^{k} tr(W_o(A,C_i)). \tag{24}$$

Therefore, the optimal locations of M sensors can be easily determined by calculating all $tr(W_o)$'s with 1 sensor placed at 1 cell and selecting the largest M of them. For λ_{min}, it has been proven to be submodular in [15]. Hence a sub-optimal solution can be found using the classic greedy algorithm, and is guaranteed to be within a certain bound of the optimum. In this paper, however, exhaustive search is still employed to find the optimal sensor locations under λ_{min} to guarantee the accuracy of analysis on optimal sensor deployment patterns.

4 RESULTS AND DISCUSSION

In this section, the results of sensor deployment using the aforementioned two metrics are presented and discussed for scalable battery systems with different sizes. First, the influence of number of sensors on the optimal $tr(W_o)$ and $\lambda_{min}(W_o)$ is analyzed and compared. Then the patterns of optimal sensor deployment under the two metrics are extracted from the results and explained by correlating to the physics of the battery system. Finally, the influences of several key system parameters, i.e. cell to cell heat conduction resistance(R_{cc}) and cell spacing(S_T), on the results are discussed.

4.1 Influence of number of sensors on observability

The optimal $tr(W_o)$ and $\lambda_{min}(W_o)$ of a 4×4 battery system under different number of sensors are plotted in Fig. 3. It is seen that both metrics are improved as the number of sensors increases. This is intuitive as more measurements means the capability to detect more energy/information in the output, hence yielding stronger observability of the states from the output. The more interesting observation is that the two metrics demonstrate different trends over the increase of sensors. Specifically, $tr(W_o)$ increases almost linearly with the number of sensors. The reason is attributed to the aforementioned modular property of $tr(W_o)$ shown in Eqn. (19), where the total $tr(W_o)$ under multiple sensors equals to the sum of $tr(W_o)$ under each one of them. Therefore, addition of sensors will lead to a near-linear increment of $tr(W_o)$, as $tr(W_o)$ under a single sensor anywhere in the pack is in

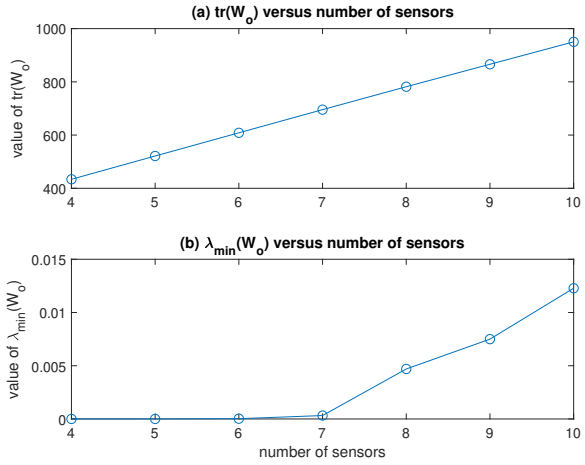

FIGURE 3: Influence of number of sensors on two metrics for a 4×4 battery system: (a) trace of observability Gramian, (b) smallest eigenvalue of Gramian

.

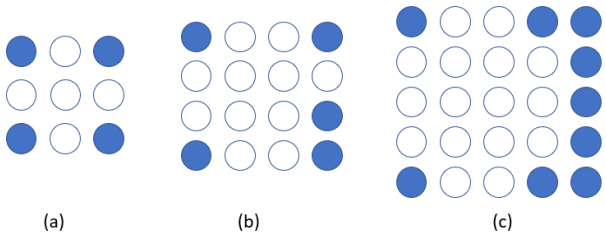

FIGURE 4: Pattern of optimal sensor deployment obtained by optimizing $tr(W_o)$, (R_{cc}=2.1 KW^{-1}, S_T=1.5): (a) 3×3 pack with 4 sensors, (b) 4×4 pack with 5 sensors,(c) 5×5 pack with 9 sensors.

the same order of magnitude. Meanwhile, $\lambda_{min}(W_o)$ is in a highly nonlinear relationship with the number of sensors as shown in Fig. 3(b), since this metric does not satisfy the modular property (but rather submodular).

4.2 Patterns of Optimal Sensor Deployment

Under the metric $tr(W_o)$, the optimal sensor locations for battery systems with sizes 3×3, 4×4, and 5×5 are shown in Fig. 4. It is interesting to note that the sensors are all located at the corners or edges of the packs. Same trend is observed for packs with larger or smaller sizes.

This pattern can be explained by exploring the unique structure of the observability gramian in the context of battery thermal system. Specifically, it is known that for two matrices G and H, we have $tr(GH) = tr(HG)$, if both GH and HG stand. Therefore, $tr(W_o)$ defined in Eqn. (19) can be rewritten as

$$\begin{aligned} \mathrm{tr}\,(W_o) &= tr\left(\int_0^\infty (e^{A^T t}C^T)(Ce^{At})dt\right) \\ &= tr\left(\int_0^\infty (Ce^{At})(e^{A^T t}C^T)dt\right) \\ &= tr\left(C\int_0^\infty e^{At}e^{A^T t}dtC^T\right) \\ &= tr(CXC^T), \end{aligned} \tag{25}$$

where

$$X = \int_0^\infty e^{At}e^{A^T t}dt \tag{26}$$

is a square matrix with a dimension of the size of the pack. It is noted that since C takes the form in Eqn. (15), $tr(CXC^T)$ is equal to the sum of the even diagonal elements of X that are specified by the sensor locations. For example, if the sensors are located at the first and second cells, $tr(CXC^T)$ is equal to the sum of the 2nd and 4th diagonal elements of X. Therefore, finding the optimal sensor locations to maximize $tr\,(W_o)$ is simply to pick the largest diagonal elements of X in the even rows, which are determined by the structure of the system matrix A. This provides insight on why optimal sensors tend to locate at the edges of the pack. It is noted that the A matrix in Eqn. (13) is diagonally dominant, as the magnitude of the diagonal elements are larger than or equal to the sum of the magnitude of other elements in the same row. Therefore, the diagonal elements of the matrix exponential e^{At} and hence $X = \int_0^\infty e^{A^T\tau}e^{A\tau}d\tau$ are largely determined by the diagonal elements of A. In this way, the sensor deployment problem is equivalent to picking the largest even diagonal elements of A. As shown in Eqn. (13), the even diagonal elements of A take the form

$$A_{ii} = \frac{-1}{C_s}\left(\frac{2}{R_u} + \frac{1}{R_c} + \frac{N}{R_{cc}}\right), \quad i = 2,4,\ldots \tag{27}$$

where N is the number of adjacent cells, i.e. $N = 2$ for cells at the corners, $N = 3$ for the other cells in the first and last rows, and $N = 4$ for cells in the middle of the pack. Consequently, cells at corners and edges are associated with larger diagonal elements as compared to those in the middle, hence being selected to maximize $tr(W_o)$.

Under the metric $\lambda_{min}(W_o)$, the optimal sensor locations for battery systems with sizes 3×3, 4×4, and 5×5 are shown in Fig. 5. It is interesting to note that the pattern is quite different from the previous case under $tr(W_o)$. Instead of locating at the edges,

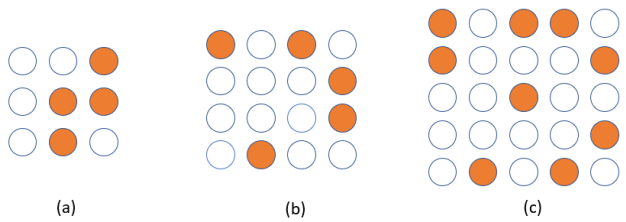

FIGURE 5: Pattern of optimal sensor deployment by optimizing $\lambda_{min}(W_o)$ (R_{cc}=2.1 KW^{-1}, S_T=1.5): (a) 3×3 pack with 4 sensors, (b) 4×4 pack with 5 sensors,(c) 5×5 pack with 9 sensors.

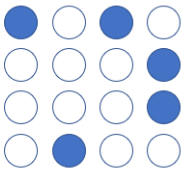

FIGURE 6: Example pack configuration and sensor locations for comparing influence of R_{cc} and S_T

the optimal sensor locations tend to distribute more evenly across the pack. This pattern can be explained by the fact that $\lambda_{min}(W_o)$ represents the observability of the least observable direction in the state space. If the sensors are concentrated in certain areas of the pack, the temperature of the cells in other parts of the pack are poorly monitored, leading to certain extremely unobservable directions in the state space. For example, if the sensors are all distributed at the edges of the pack, as in the previous case to optimize $tr(W_o)$, overheating of the middle cells will be poorly observable. Therefore, even distribution of sensors appears to be the best strategy to avoid any potential extreme worst cases.

4.3 Influence of R_{cc} and S_T on two metrics

In this section, the influence of critical pack parameters on system observability is investigated, including cell to cell heat conduction resistance R_{cc} and cell spacing S_T. These two parameters reflect the thermal interconnection between cells, and are important control-related parameters to be considered in battery pack design. The optimal $tr(W_o)$ and $\lambda_{min}(W_o)$ over a range of R_{cc} and S_T for a 4×4 battery pack with 5 sensors deployed as in Fig. 6 are shown in Fig. 7 for illustration.

For R_{cc}, as shown in Fig. 7(a), the optimal value of $tr(W_o)$ increases monotonically with R_{cc}, which can be explained by the structure of $tr(W_o)$. As has been discussed in the previous section, $tr(W_o)$ is strongly correlated with the even diagonal elements of the A matrix, i.e. A_{ii} as shown in Eqn. (27). Then it is apparent that as R_{cc} increases, A_{ii} will increase as it contains a $-1/R_{cc}$ term. Therefore, higher R_{cc} yields better average observability in the sense of the trace of observability gramian. Meanwhile, $\lambda_{min}(W_o)$ shows a nonmonotonic trend over varying R_{cc} according to Fig. 7(b). The peak value of $\lambda_{min}(W_o)$ is attained at a certain R_{cc}, which is dependent on configuration and other parameters of the battery pack. This interesting observation points to the possibility/need of designing R_{cc} to optimize the worst-case system observability in the sense of $\lambda_{min}(W_o)$.

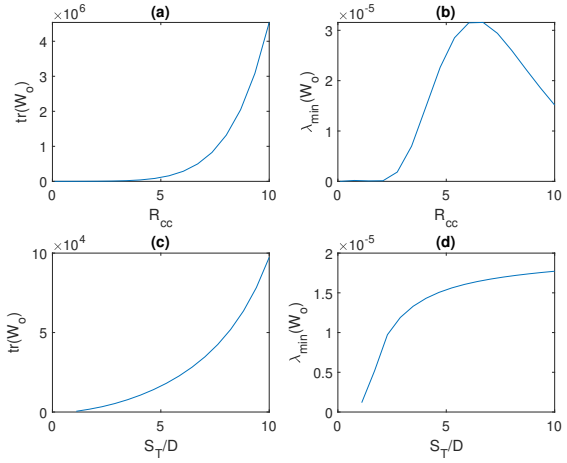

FIGURE 7: Impact of R_{cc} and S_T on $tr(W_o)$ and $\lambda_{min}(W_o)$

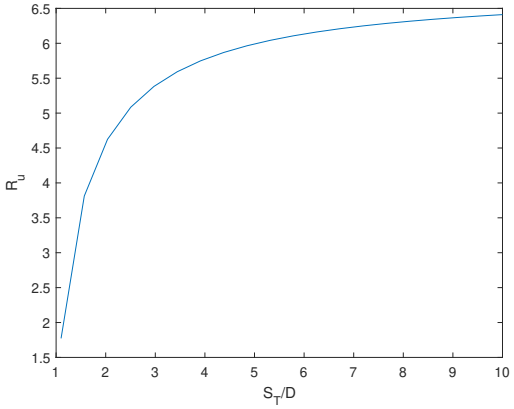

FIGURE 8: Relation between heat convection resistance R_u and cell spacing S_T

For S_T, as shown in Fig. 7(c), the relation between S_T and $tr(W_o)$ is also monotonic similar to the influence of R_{cc}. According to Eqn. (2-7), R_u is positively correlated to S_T as plotted in Fig. 8. Since A_{ii} contains a term $-2/R_u$ as in Eqn. (27), larger R_u leads to higher value of A_{ii}, which means higher average observability. Meanwhile, $\lambda_{min}(W_o)$ is also in a monotonically increasing relationship with S_T as shown in Fig. 7(d).

5 CONCLUSION

In this paper, temperature sensor deployment for scalable battery packs is studied. First, a scalable battery pack model including the thermal interconnection between cells is developed to capture the battery pack thermal dynamics. Optimal sensor locations are then found in terms of two Gramian-based observability criteria, i.e. $tr(W_o)$ and $\lambda_{min}(W_o)$, which quantify the average and worst-case system observability respectively. Optimal sensor deployment patterns are then extracted from the results which are generalizable to battery packs of varying sizes. Specifically, placing sensors at the edges of the pack results in higher overall/average system observability in the sense of $tr(W_o)$, whereas distributing sensors more evenly in the battery pack can ensure better worst-case observability in the sense of $\lambda_{min}(W_o)$. Furthermore, better average observability can be obtained by either increasing the cell to cell heat conduction resistance R_{cc} or enlarge the spacing between cells S_T. Meanwhile, worst-case observability can be improved by increasing S_T or placing R_{cc} at the optimal value which depends on pack configuration and parameters.

REFERENCES

[1] Park, C., and Jaura, A. K., 2003. Dynamic thermal model of li-ion battery for predictive behavior in hybrid and fuel cell vehicles. Tech. rep., SAE Technical Paper.

[2] Jangra, S., Chung, C. H., Lai, Q., and Lin, X., 2019. "Optimal maintenance of electric vehicle battery system through overnight home charging". In ASME 2019 Dynamic Systems and Control Conference, American Society of Mechanical Engineers Digital Collection.

[3] Michel, N., Sinha, A. K., Kong, Z., and Lin, X., 2019. "Multiphysical modeling of energy dynamics for multirotor unmanned aerial vehicles". In 2019 International Conference on Unmanned Aircraft Systems (ICUAS), IEEE, pp. 738–747.

[4] Marsh, R., Vukson, S., Surampudi, S., Ratnakumar, B., Smart, M., Manzo, M., and Dalton, P., 2001. "Li ion batteries for aerospace applications". *Journal of power sources,* **97**, pp. 25–27.

[5] Lin, X., Kim, Y., Mohan, S., Siegel, J. B., and Stefanopoulou, A. G., 2019. "Modeling and estimation for advanced battery management". *Annual Review of Control, Robotics, and Autonomous Systems,* **2**, pp. 393–426.

[6] Lin, X., Fu, H., Perez, H. E., Siege, J. B., Stefanopoulou, A. G., Ding, Y., and Castanier, M. P., 2013. "Parameterization and observability analysis of scalable battery clusters for onboard thermal management". *Oil & Gas Science and Technology – Revue d'IFP Energies nouvelles,* **68**(1), jan, pp. 165–178.

[7] Abdul Samad, N., 2016. "Improved battery state estimation using novel sensing techniques.". PhD thesis, University of Michigan.

[8] Tian, N., Fang, H., and Wang, Y., 2017. "3-d temperature field reconstruction for a lithium-ion battery pack: A distributed kalman filtering approach". *IEEE Transactions on Control Systems Technology,* **27**(2), pp. 847–854.

[9] Lin, X., Stefanopoulou, A. G., Siegel, J. B., and Mohan, S., 2014. "Temperature estimation in a battery string under frugal sensor allocation". In ASME 2014 Dynamic Systems and Control Conference, American Society of Mechanical Engineers Digital Collection.

[10] Lin, X., Perez, H. E., Siegel, J. B., and Stefanopoulou, A. G., 2019. "Robust estimation of battery system temperature distribution under sparse sensing and uncertainty". *IEEE Transactions on Control Systems Technology*.

[11] Lin, X., 2014. "Adaptive estimation of thermal dynamics and charge imbalance in battery strings.". PhD thesis, University of Michigan.

[12] Lystianingrum, V., Hredzak, B., Agelidis, V. G., and Djanali, V. S., 2014. "Observability degree criteria evaluation for temperature observability in a battery string towards optimal thermal sensors placement". *2014 IEEE Ninth International Conference on Intelligent Sensors, Sensor Networks and Information Processing (ISSNIP)*.

[13] Wolf, P., Moura, S., and Krstic, M., 2012. "On optimizing sensor placement for spatio-temporal temperature estimation in large battery packs". In 2012 IEEE 51st IEEE Conference on Decision and Control (CDC), IEEE, pp. 973–978.

[14] Lin, X., Perez, H. E., Siegel, J. B., Stefanopoulou, A. G., Li, Y., Anderson, R. D., Ding, Y., and Castanier, M. P., 2012. "Online parameterization of lumped thermal dynamics in cylindrical lithium ion batteries for core temperature estimation and health monitoring". *IEEE Transactions on Control Systems Technology,* **21**(5), pp. 1745–1755.

[15] Summers, T. H., Cortesi, F. L., and Lygeros, J., 2015. "On submodularity and controllability in complex dynamical networks". *IEEE Transactions on Control of Network Systems,* **3**(1), pp. 91–101.

[16] Mahamud, R., and Park, C., 2011. "Reciprocating air flow for li-ion battery thermal management to improve temperature uniformity". *Journal of Power Sources,* **196**(13), pp. 5685–5696.

[17] Bergman, T. L., Incropera, F. P., DeWitt, D. P., and Lavine, A. S., 2011. *Fundamentals of heat and mass transfer*. John Wiley & Sons.

[18] Smith, K., Kim, G.-H., Darcy, E., and Pesaran, A., 2010. "Thermal/electrical modeling for abuse-tolerant design of lithium ion modules". *International Journal of Energy Research,* **34**(2), pp. 204–215.

[19] Chen, C.-T., 1998. *Linear system theory and design*. Oxford University Press, Inc.